atmosphere

MDPI

Article

Scenario-Based Assessment of Urban Heat-Stress Risk in Vilnius, Lithuania

Justina Kapilovaitė and Egidijus Rimkus *

Institute of Geosciences, Vilnius University, LT-03225 Vilnius, Lithuania; justina.kapilovaite@chgf.stud.vu.lt
* Correspondence: egidijus.rimkus@gf.vu.lt

Abstract

Urban areas are increasingly exposed to heat stress under climate change due to rising temperatures, ageing populations, and increasing population density in cities. This study assesses current and future heat-stress risk in Vilnius, Lithuania, using the Humidex index and the CLIMADA risk modelling framework. Historical heat-stress conditions are analysed using observational meteorological data, while future conditions are evaluated using five CMIP6 climate models under SSP2-4.5 and SSP5-8.5 climate scenarios for the mid and late 21st century. The risk assessment combines high-resolution Humidex-based hazard data, gridded population exposure, and age-specific vulnerability functions. In addition to temporal Humidex trend analysis, CLIMADA is used to estimate spatially explicit Expected Annual Impact and population-normalised impact indicators. The frequency of heat-induced stress has increased significantly—the number of days when the Humidex index was $\geq$30 has risen by 5.6 days per decade. It is projected that by the end of the century, the proportion of such warm-season days (April–October) will increase from 13.1% to 25.8% under the SSP2-4.5 scenario and to 41.6% under the SSP5-8.5 scenario. Spatial impact maps identify areas with elevated total and population-normalised heat-stress burden, while age-specific results show higher impacts among residents aged $\geq$ 65 years. Cumulative heat-stress burden, expressed as Expected Annual Impact, could increase by approximately 1.8–11.4 times. The framework provides a spatially consistent and age-sensitive approach for assessing urban heat-stress risk and supporting local climate adaptation planning.

Keywords: climate risk assessment; heat-stress; urban areas; humidex; population exposure; vulnerability functions; spatial risk mapping

Check for updates

Academic Editors: Ferdinando Salata and A. Santos Nouri

Received: 22 June 2026
Revised: 21 July 2026
Accepted: 28 July 2026
Published: 30 July 2026

Copyright: © 2026 by the authors. Licensee MDPI, Basel, Switzerland. This article is an open access article distributed under the terms and conditions of the Creative Commons Attribution (CC BY) license.

1. Introduction

Climate change is altering global temperature patterns and increasing the frequency and intensity of extreme heat events in urban areas [1]. Northern and Eastern European cities, such as Vilnius, Lithuania, are experiencing pronounced shifts in temperature regimes and heatwave characteristics [2,3]. Anthropogenic climate change, combined with rapid urbanisation and population ageing, creates a complex landscape in which urban residents, especially those in vulnerable groups, face greater exposure to extreme heat [4]. According to the Lancet Countdown on health and climate change, in 2019, vulnerable populations worldwide were exposed to an additional 475 million heatwave events, representing a critical escalation in heat exposure [5]. There has been a 53.7% increase in heat-related mortality in people older than 65 years over the past two decades, resulting in approximately 296,000 deaths in 2018 alone [5].

Climate models are widely used to assess how future meteorological conditions may change under different greenhouse-gas emission scenarios. Global climate models from the CMIP6 project provide such projections for a range of Shared Socioeconomic Pathways (SSPs) [6,7]. These models' projections provide valuable insights into changes in temperature extremes and heat-related hazards under different emission scenarios [8]. However, assessing hazard alone is insufficient for understanding societal implications. The Intergovernmental Panel on Climate Change (IPCC) risk framework emphasises that understanding the implications for society requires going beyond hazard and considering how the hazard affects exposed citizens with different levels of vulnerability [9]. The IPCC specified an approach to calculate risk by assessing vulnerability (sensitivity and capacity of exposed populations/assets to adapt to a hazard), exposure (the spatial distribution of populations or assets potentially in danger of a hazard), and hazard (the intensity and frequency of extreme weather events) [9,10].

Several publicly available, open-source frameworks have been developed for assessing natural hazards and climate-related risks, including CLIMADA [11], Oasis Loss Modelling Framework [12], RiskScape [13] and VIGIRISKS [14]. Among these, CLIMADA (CLIMate ADAptation) is particularly suitable for this study because it provides a flexible, transparent, and event-based framework for combining hazard, exposure, and vulnerability components to estimate climate-related impacts [11,15–17].

Within climate impact modelling frameworks, hazards can be defined by thermal indices, such as Humidex, Wet-Bulb Globe Temperature (WBGT), and Universal Thermal Climate Index (UTCI) [18–22]. These indices combine temperature with humidity, solar radiation, or wind speed, providing a more accurate assessment of thermal stress conditions and better calculation of impacts relevant to humans. Thermal indices provide a more suitable representation of heat-related hazards than temperature alone and have been used to assess heat-related mortality, work capacity and other impacts [23–26].

Although heatwaves and heat-stress risks are receiving increasing attention across Europe, the Baltic States still lack comprehensive studies that integrate thermal indices with the hazard, exposure and vulnerability framework. Prior research in Baltic countries (Lithuania, Latvia, Estonia) has predominantly investigated heat extremes as separate phenomena, focusing on temperature trends or projections [2,3,27–31]. As a result, the combined effects of rising heat intensity, population distribution and vulnerability have not been comprehensively assessed within the Baltic region. Furthermore, high-resolution urban-scale assessments in Baltic cities are lacking. Existing heat assessments are based on regional climate model data (12.5 km) and tend to yield results that are too coarse to understand heat exposure at the urban scale [2,28,30].

This study aims to assess future urban heat-stress risk under climate change scenarios for the municipality of Vilnius, Lithuania. The study uses the CLIMADA model to quantify heat-stress risk for Vilnius citizens, using a high spatial-resolution (100 m) Humidex index as the hazard, incorporating age-dependent vulnerability functions, and population distribution as the exposure. Unlike previous studies that focus on working capacity or mortality, this study emphasises population-level heat-stress responses and provides a spatially consistent assessment of heat-stress risk in urban areas.

2. Materials and Methods

2.1. Study Area

The study area is defined as the entire Vilnius city municipality, located in southeastern Lithuania (Figure 1). The city lies at approximately 54.687° N and 25.280° E, at an elevation ranging from 97 m to 233 m above sea level. The administrative area of Vilnius covers 401 km^2 and is characterised by a glacially formed landscape of undulating plains and

river valleys. Population density is uneven across the municipality, with the highest concentrations generally found in densely built residential districts. At the sub-municipal administrative level, density ranges from 113 residents to 8721 residents km^{-2}, reflecting the contrast between compact urban districts and peripheral, forested, and less urbanised areas (2021 data) [32]. Approximately 47% of the city's area is covered by forests and other vegetated land, including semi-forest, dense forest and green urban areas (2019 data) [33]. The population of Vilnius is 607,984 as of 2025, of whom approximately 17.5% are aged 65 and older.

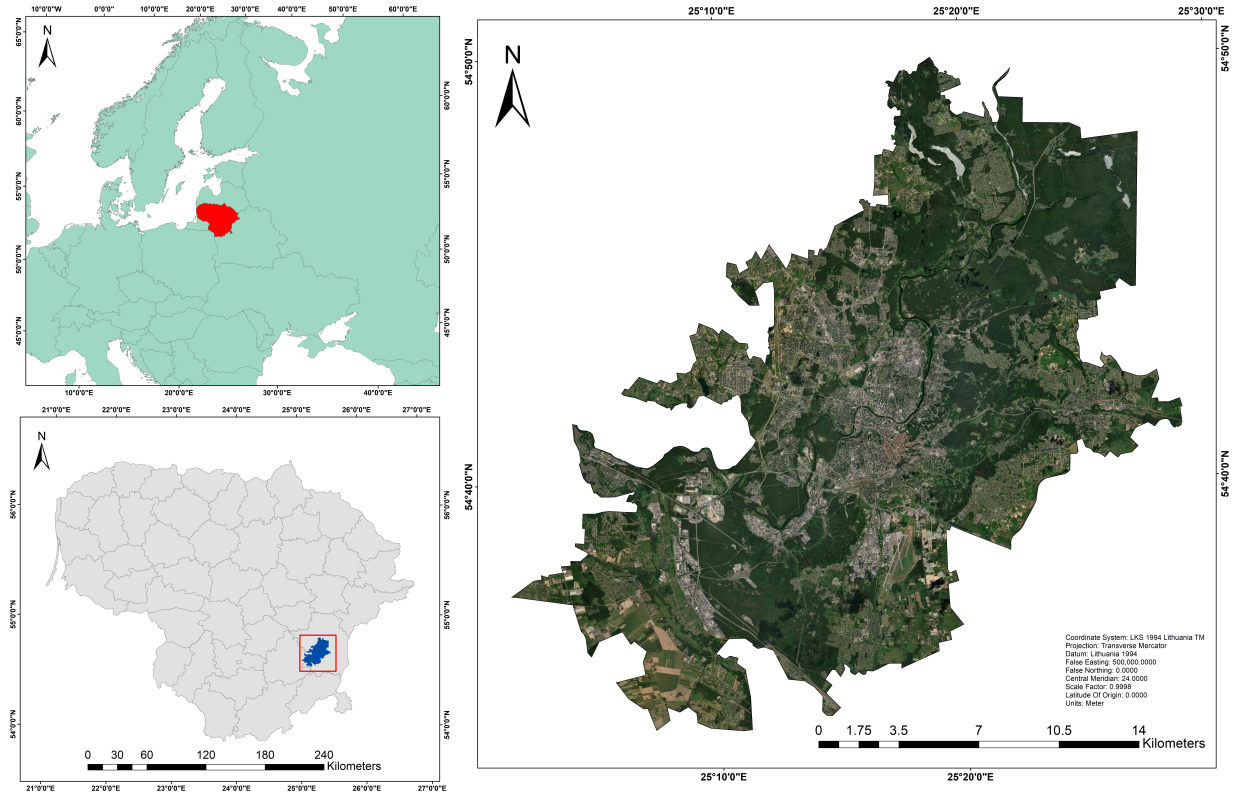

Figure 1. Study area: Vilnius, Lithuania. The top-left inset shows Lithuania within Europe, and the bottom-left inset shows Vilnius within Lithuania. The main panel shows the administrative territory of Vilnius overlaid on a true-colour remotely sensed image, illustrating the spatial distribution of built-up areas, vegetation, and water bodies.

According to the Köppen–Geiger climate classification, Vilnius is classified as Dfb (humid continental climate), characterised by cold winters and warm summers. Over the period 1991–2020, the mean annual air temperature in Vilnius was 7.2 °C. The mean temperature of the coldest month is −3.7 °C, while the warmest month averages 18.5 °C. The city receives an average of 674 mm of precipitation per year, with the maximum in summer. During the 1991–2020 reference period, the city recorded an average of 5.1 days per year with a maximum temperature above 30 °C, which is particularly relevant for assessing urban heat stress and adaptation needs in Vilnius.

2.2. Data and Methods

2.2.1. Methodological Overview

This research assesses the current and future risks of urban heat stress in Vilnius, Lithuania, under different climate change scenarios, and evaluates the overall impacts of heat stress across age groups within the urban population. A detailed methodological framework for assessing climate-related risks was developed by combining three key risk elements: hazard, exposure, and vulnerability. The assessment utilised the CLIMADA

platform. The hazard aspect was represented by the Humidex index, chosen for its ability to better capture the perceived heat stress experienced by individuals. Hazard datasets based on the Humidex index were prepared for the CLIMADA model to analyse both current and future climate. In addition to the modelling approach, an independent analysis of historical Humidex data was conducted to examine long-term trends and changes in heat-stress perception in Vilnius. The exposure component focused on mapping the distribution of the urban population by age group and location across the city. Vulnerability was assessed by developing age-specific vulnerability functions that reflect varying sensitivities to heat stress.

2.2.2. Hazard

The hazard assessment in this research utilised the Humidex index as the primary heat-stress indicator. By considering both air temperature and humidity, this index effectively assesses human thermal discomfort and identifies potential heat-related risks to the public. Observational data for the present climate period (1991–2024) were obtained from the Lithuanian Hydrometeorological Service (LHMS) for the Trakų Vokė meteorological station, representing the Vilnius area. The Trakų Vokė meteorological station was used only as the reference meteorological station. Spatial variations in air temperature and humidity across Vilnius were represented by applying high-resolution (100 m $\times$ 100 m) UrbClim anomaly fields to the station observations. The analysis used daily maximum air temperature (T_{max}) and relative humidity (RH) observations recorded at 13 UTC. This observation time was selected because it generally coincides with the period of highest daytime thermal stress. The full observational period 1991–2024 was analysed separately to evaluate long-term historical changes in Humidex conditions, while the 2001–2020 subset was used as the present-climate reference period in the CLIMADA impact assessment to ensure consistency with the 20-year future projection periods.

Future climate projections were derived from NASA Earth Exchange Global Daily Downscaled and Bias-Corrected CMIP6 Projections with a spatial resolution of 0.25° $\times$ 0.25° under the SSP2-4.5 and SSP5-8.5 climate scenarios [34,35]. Five CMIP6 models were selected to represent a range of climate sensitivities and possible future climate responses: Canadian Earth System Model version 5 (CanESM5), Australian Community Climate and Earth-System Simulator Coupled Model version 2 (ACCESS-CM2), Geophysical Fluid Dynamics Laboratory Climate Model version 4 (GFDL-CM4), Max Planck Institute Earth System Model version 1.2, low resolution (MPI-ESM1-2-LR), and Norwegian Earth System Model version 2, medium resolution (NorESM2-MM) [36]. For brevity, the shortened model names CanESM, ACCESS, GFDL, MPI, and NorESM are used in the following sections and figures.

Two future periods were assessed: 2041–2060 and 2081–2100. All calculations were performed for the warm season (April–October). The CMIP6 baseline period 1991–2014 was selected because it overlaps with the available LHMS observations and CMIP6 historical simulations, prior to the start of the SSP projections in 2015 [35]. This baseline was used to compare modelled Humidex exceedance frequencies with LHMS observations and to assess whether additional bias adjustment was required. The comparison showed broadly similar exceedance frequencies for Humidex $\geq$30 and $\geq$35, with observed values of 11.4% and 3.45%, respectively, compared with model ranges of 10.0–13.6% and 2.30–3.95%. For the rarer Humidex $\geq$40 and $\geq$45 categories, absolute exceedance frequencies remained low across all datasets, ranging from 0.14% to 0.82% and from 0.00% to 0.12%, respectively. Therefore, additional bias adjustment was not applied in this study.

In this study, both the observational and CMIP6 climate datasets represented the Vilnius region using a single spatial point. Observational data were obtained from the Trakų

Vokė meteorological station, while the CMIP6 projections were available at a relatively coarse spatial resolution of 0.25° × 0.25°. As these datasets were insufficient to capture the spatial variability of heat-stress conditions across the city, high-resolution UrbClim simulations were incorporated to better represent the spatial distribution of heat stress within Vilnius [37]. UrbClim is a specialised urban climate model that focuses on replicating urban climate patterns in detail, usually down to a hundred-metre scale. This model integrates principles of urban physics with a 3-D atmospheric boundary-layer component. It characterises urban surfaces as rough, impermeable slabs with unique properties like albedo, emissivity, thermal conductivity, and volumetric capacity [37,38]. Data from UrbClim for Vilnius between 2008 and 2017, with a spatial resolution of 100 × 100 m, were used [37]. The study utilised daily maximum 2 m temperature, daily average 2 m temperature, and daily mean specific humidity at 2 m.

Humidex was calculated to represent near-maximum daily heat-stress conditions following the approach of Masterton and Richardson (1979) [39]:

$$Humidex = T_{max} + \frac{5}{9}(e - 10) \quad (1)$$

where T_{max} is the maximum air temperature (°C) and e is the vapour pressure (hPa). Vapour pressure was required for the Humidex calculation, but was not directly available in all datasets. Therefore, it was derived from available humidity variables using standard meteorological equations before the Humidex calculation to ensure methodological consistency. For the observational and CMIP6 datasets, vapour pressure was calculated from relative humidity using the saturated vapour pressure formulation based on the H. Magnus (1844) equation [40]. For the UrbClim dataset, vapour pressure was derived from specific humidity, assuming a constant atmospheric pressure of 1000 hPa.

To characterise intra-urban heat-stress patterns during hot conditions, days with maximum air temperature ≥30 °C at the Trakų Vokė meteorological station were selected. For these hot-event days, UrbClim temperature and specific humidity data were averaged, and specific humidity was converted to vapour pressure. Spatial anomalies in air temperature and vapour pressure were then calculated for each UrbClim grid cell relative to the UrbClim grid cell corresponding to the Trakų Vokė reference location.

$$\Delta T = T_{grid} - T_{obs} \quad (2)$$

$$\Delta e = e_{grid} - e_{obs} \quad (3)$$

where T_{grid} and e_{grid} represent UrbClim grid-cell temperature and vapour pressure values, while T_{obs} and e_{obs} correspond to Trakų Vokė meteorological station values used as the reference location (Figure 2). The average anomaly values were then used to create spatially distributed datasets of temperature, vapour pressure, and Humidex across Vilnius by applying them to individual observational points and CMIP6 model datasets. Figure 2 shows the available UrbClim model domain, which does not fully cover the Vilnius administrative boundary. Areas outside the domain were assumed to have the same temperature as that at the Trakų Vokė meteorological station, with the temperature difference set to 0.

This approach assumes that the present-day spatial structure of the urban heat island remains constant over the future projection periods. This assumption reflects the study's scope, which focuses on climate-driven changes in heat-stress risk within Vilnius's current spatial structure. Future possible changes in urban morphology, land cover, greening, building density, and urban expansion were not considered. The implications and limitations of this assumption are discussed further in Sections 4.3 and 4.6. The derived datasets were resampled to the 250 m × 250 m population grid using average resampling and clipped to

the Vilnius City Municipality boundary, ensuring matching grid alignment and cell centroids for the CLIMADA analysis. Only days during which at least 50% of valid grid cells exceeded a Humidex threshold of 30 °C were classified as heat-stress events and included in the Expected Annual Impact (EAI) calculations within the CLIMADA risk assessment framework. The 50% threshold was selected to represent city-wide heat-stress conditions rather than localised hotspots affecting only a small part of the municipality. Using a higher Humidex threshold would reduce the absolute EAI values because fewer heat-stress events would be included, while the relative differences among periods, scenarios, and age groups are expected to remain broadly consistent. This study does not account for the cumulative impact of prolonged severe heat stress, which can lead to more severe outcomes than isolated instances.

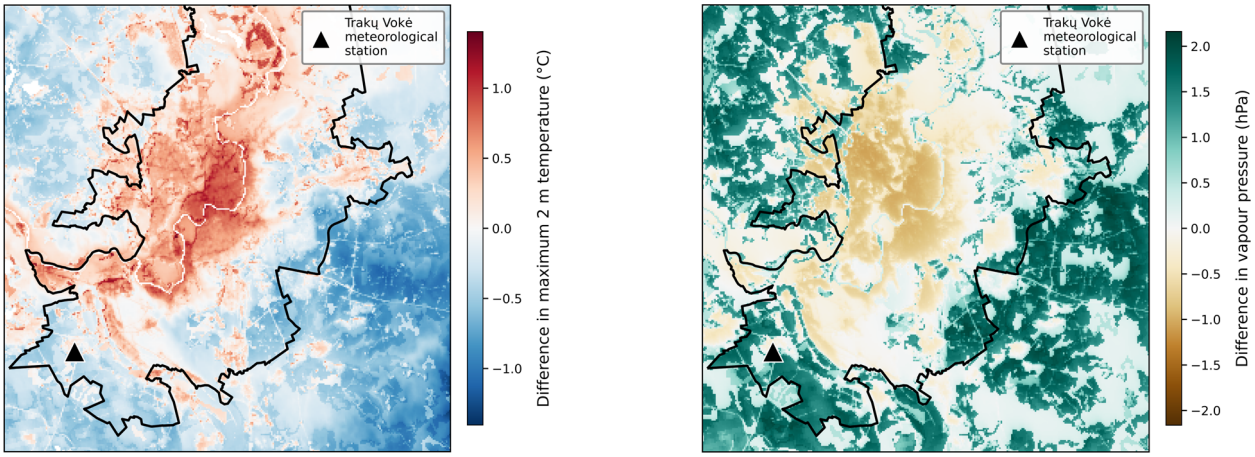

(**a**) (**b**)

Figure 2. Mean April–October spatial anomalies relative to Trakų Vokė meteorological station across Vilnius during hot-event days ($T_{max} \geq 30$ °C), derived from UrbClim simulations for the 2008–2017 period: (**a**) daily maximum 2 m air temperature anomalies (°C); (**b**) vapour pressure anomalies (hPa).

In addition to the climate risk modelling framework, a separate historical Humidex analysis was conducted using observational data for the 1991–2024 period to evaluate long-term changes in perceived heat stress in Vilnius. Heat-stress days were classified into four categories based on Humidex values: 30–<35, 35–<40, 40–<45, and ≥45. These thresholds follow Environment and Climate Change Canada guidance, with 35 included as an additional analytical threshold within the broader 30–39 discomfort range [41]. Linear regression, combined with the Mann–Kendall trend test ($p < 0.05$), was utilised to evaluate trends in the annual occurrence of Humidex values equal to or exceeding 30, 35, and 40. In contrast, Poisson regression was applied to analyse Humidex values of 45 or higher, given the data's discrete nature.

2.2.3. Exposure

Exposure in climate risk assessments refers to the spatial configuration and characteristics of entities vulnerable to hazards. In this study, exposure assessment was based on spatial population grid data from the Lithuanian State Data Agency, with a resolution of 250 m × 250 m. The obtained 2021 dataset included population distribution by age groups and was aggregated into three demographic categories associated with differing heat-stress sensitivities: children (0–14 years), working-age population (15–64 years), and elderly population (65+ years). The exposure values used in the climate-risk calculations represented the absolute number of residents in each grid cell for each age group, rather than the proportion of an age group within the total population.

To maintain coherence in climate risk evaluations across different time periods, the initial spatial population dataset from 2021 was reconfigured to incorporate past demographic data and population forecasts from the Lithuanian State Data Agency. For historical assessment, population totals were adjusted to the mean population values for the analysed period (2001–2020). For future assessments, the total population of Vilnius City Municipality in 2025 (607,667 inhabitants) was adopted as the baseline population and assumed to remain constant until 2100. This constant-population assumption was selected because historical demographic data show that Vilnius City Municipality's population has not followed the national declining trend in a linear manner. After decreasing from 578,327 residents in 1996 to 535,362 in 2014, the population increased to 607,667 in 2025, consistent with broader urbanisation trends in which major cities may continue to attract population despite national-level decline [42–44]. However, spatially explicit long-term population projections for Vilnius City Municipality were not available. Therefore, keeping the 2025 population constant was considered a neutral assumption that avoids speculative estimates of future population growth, decline, or intra-urban redistribution while allowing the assessment to focus on climate-driven changes in heat-stress risk.

Population age-group composition for each assessment period was adjusted using national demographic projections from the Lithuanian State Data Agency, representing the percentage distribution of age groups within the total population. For future periods, 20-year mean age-group percentage distributions were calculated and applied to the baseline spatial population dataset. These percentages were used to calculate the corresponding absolute population counts for each age group in every grid cell. While the overall age-group distribution varied across assessment periods, the relative spatial distribution of the population within individual grid cells remained unchanged and was preserved according to the original 2021 dataset.

Figure 3 presents an example of the spatial population datasets used for the historical climate-risk assessment during the 2001–2020 period, including total population distribution and the relative share of the elderly population across Vilnius. White grid cells represent unpopulated areas, primarily forests, parks, water bodies, and other non-residential land-use types.

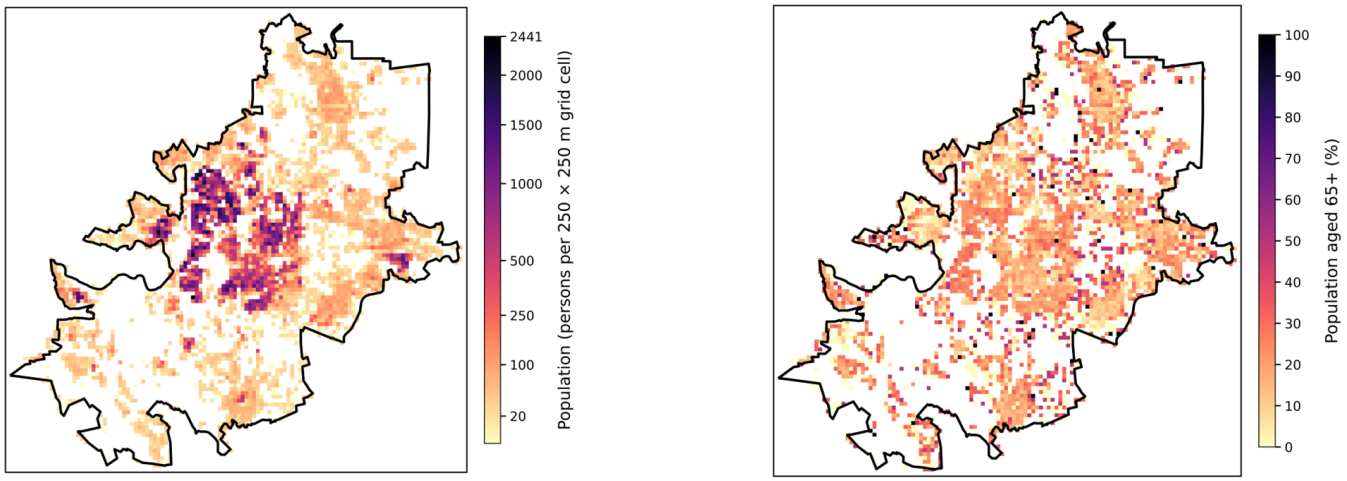

Figure 3. Spatial distribution of population exposure characteristics in Vilnius during the 2001–2020 period: (**a**) mean total population count per grid cell across all age groups; (**b**) mean share of elderly population (65+ years) within individual population grid cells.

2.2.4. Vulnerability

Within the CLIMADA framework, vulnerability represents the sensitivity of the exposed population to the analysed hazard and is described using vulnerability functions that relate hazard intensity to the resulting impact level. This impact is measured using the Mean Damage Ratio (MDR), which is derived from the mean damage degree (MDD) and the percentage of the exposed population affected by the hazard. In this study, the percentage of affected assets was assumed to be 100%, meaning that the entire exposed population was considered potentially affected during heat-stress events.

In this study, vulnerability functions illustrate the relationship between Humidex intensity and the relative heat-stress burden experienced by the population. This study's objective was not to directly quantify mortality, morbidity, or physical working capacity. Instead, we developed a generalised heat-stress burden function using the sigmoid-shaped methodological framework proposed by Foster et al. [22]. This vulnerability function enables a gradual increase in heat-stress impact as Humidex intensity rises, while also ensuring that the response remains within theoretical lower and upper limits (Figure 4).

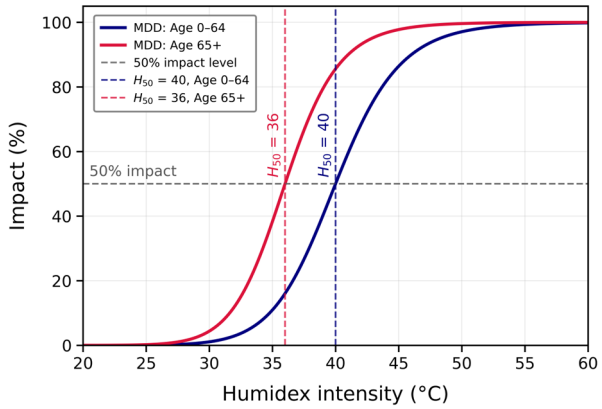

Figure 4. Mean Damage Degree (MDD) functions used to represent heat-stress vulnerability for different population age groups as a function of Humidex intensity. The *x*-axis represents Humidex intensity (°C), while the *y*-axis represents relative heat-stress impact (%).

The vulnerability functions were parameterised based on previous studies investigating heat-related mortality risk and thermal stress responses [24]. However, since this study aimed to evaluate the overall population-level burden of heat stress rather than specific health, mortality or work-related outcomes, the vulnerability thresholds were adjusted to reflect thermal discomfort and perceived heat burden among the Vilnius population.

For the working-age population and children, the midpoint of the vulnerability response curve (H_{50}) was set at Humidex = 40. This threshold was derived by adapting relative risk relationships reported in previous heat-mortality studies to represent generalised heat-stress burden conditions rather than mortality outcomes [24]. The selected threshold corresponds to conditions classified as very high thermal discomfort and substantially elevated heat stress. For the elderly population, a lower Humidex threshold of 36 was applied to reflect the greater heat sensitivity of older individuals and the earlier onset of significant thermal burden.

Vulnerability functions used in this study:

$$\mathrm{MDD}_a(H) = \frac{1}{1 + \left(\frac{H_{50,a}}{H}\right)^{n_a}}, H > 0 \quad (4)$$

where $\mathrm{MDD}_a(H)$ is the Mean Damage Degree function at age a, H is Humidex, $H_{50,a}$ represents the value of Humidex level associated with 50% heat-stress impact for age group

a, and n_a represents the gradient of the vulnerability function. For specific age groups, the parameters are given as follows: $H_{50,c} = H_{50,w} = 40$, $n_c = n_w = 15.7$; $H_{50,e} = 36$, $n_e = 16.88$, with c, w and e representing children, the working-age group population, and the elderly, respectively.

In the vulnerability assessment, children were categorised alongside the working-age population. This simplification was applied because children's heat sensitivity and adaptive capacity vary significantly across developmental stages, from infancy to adolescence, whereas this study focused on a generalised heat-stress burden rather than on detailed physiological or medical responses.

The steepness parameters of the vulnerability functions were calibrated to ensure a realistic progression of heat-stress impacts as Humidex levels increase and to maintain consistency with established Humidex thermal discomfort categories. However, these functions are theoretical, scenario-based tools intended to support relative comparisons among age groups, locations, and climate scenarios, rather than empirically calibrated effect functions. The resulting vulnerability functions should therefore be interpreted as generalised representations of relative heat-stress sensitivity and may be further refined in future studies using local epidemiological data, health statistics, and updated climate-health research for Lithuania.

2.2.5. Risk Assessment

Heat-stress risk assessment was performed within the CLIMADA framework by calculating event-based impacts at the grid-cell level and subsequently aggregating them to derive cumulative and mean annual Expected Annual Impact (EAI) metrics. Event impacts were estimated by combining local hazard intensity with the corresponding exposed population and age-specific vulnerability functions. For each selected heat-stress event, the Humidex value in each grid cell was converted into a relative impact value using the relevant age-specific vulnerability function. This value was then multiplied by the population of the corresponding age group in that grid cell.

Children and the working-age population were assigned the same vulnerability function, while the elderly population was assigned a separate function. The resulting impacts were aggregated to obtain the total impact for each spatial unit. The impacts were first summed across all valid grid cells and age groups for each selected event. Event impacts were then summed within each year to obtain the annual cumulative impact. Each selected heat-stress day contributed once to this annual total. The cumulative impact for the full study period was obtained by summing the annual impacts, while the mean annual EAI was calculated by dividing the cumulative impact by the number of years in the analysed period.

In this study, EAI represents a comparative, modelled cumulative impact indicator rather than the actual number of affected individuals or a direct estimate of health outcomes. It reflects the cumulative heat-stress burden associated with recurrent heat events over the analysed period and is expressed as the cumulative equivalent impact units. EAI values, therefore, represent cumulative equivalent impacts resulting from varying degrees of heat-stress exposure. For example, the same EAI value may result either from a smaller population experiencing severe impacts or from a larger population experiencing lower-intensity impacts over multiple heat events.

Higher EAI values, therefore, indicate areas where populations are exposed to more frequent and/or more intense heat-stress conditions, leading to greater cumulative burden. However, no empirically validated EAI thresholds are currently available. Therefore, the values should be interpreted comparatively rather than as predefined "low," "medium," or "high" burden categories. Population-normalised EAI values (per 100 inhabitants) were

additionally calculated to enable comparison of relative heat-stress burden between areas with differing population densities. Continuous colour scales were used in the maps to show the spatial variation in EAI without classifying values into burden levels.

3. Results

3.1. Historical Trends and Projected Changes in Heat-Stress Hazard

Analysis of observational data from 1991 to 2024 reveals substantial long-term variability in heat-stress frequency across multiple intensity thresholds during the April–October warm season. The frequency of days with Humidex ≥ 30 °C ranged from 7 days (1993, 2000) to 50 days (2024), demonstrating marked inter-annual fluctuations (Figure 5, left panel). More intense categories demonstrated even greater rarity and variability: days exceeding Humidex ≥ 35 °C ranged from 0 to 22 days per year, while days with Humidex ≥ 40 °C were rare before 2010 (0–2 days annually) but increased substantially in 2010 (7 days), with subsequent persistent occurrences (0–7 days annually through 2024). Extreme events (Humidex ≥ 45 °C) remained sparse, typically occurring 0–1 days per year, but showed increased frequency in recent years (2007, 2009, 2011, 2015, 2018, 2020–2024).

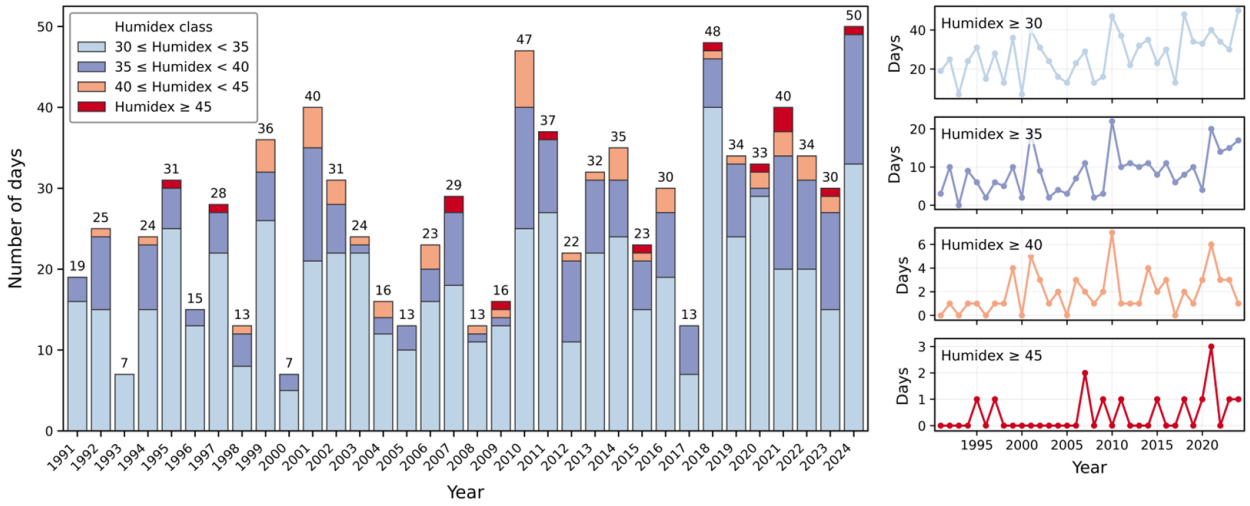

Figure 5. Annual frequency of heat-stress days by Humidex class in Vilnius during the April–October season, 1991–2024. The left panel shows the number of days per year, grouped into four Humidex categories: 30–35, 35–40, 40–45, and ≥45. The panels on the right show annual trends in the number of days exceeding selected Humidex thresholds: ≥30, ≥35, ≥40, and ≥45. The analysis is based on observational data and illustrates long-term changes in perceived heat stress in Vilnius over the historical period.

Temporal trends in annual Humidex exceedance frequency were assessed using threshold-specific statistical approaches (Figure 5, right panels). Trend analysis revealed statistically significant increases across all assessed Humidex thresholds. The largest absolute increases occurred at Humidex ≥ 30 and ≥35 °C, with increases of +5.57 and +2.64 days per decade, respectively (both $p < 0.01$). Exceedances of Humidex ≥ 40 °C also increased significantly (+0.60 days per decade, $p = 0.020$). For Humidex ≥ 45 °C, Poisson regression indicated a significant increase of +0.40 expected days per decade ($p = 0.028$). These results indicate that during the April–October warm season, Vilnius has experienced a significant increase in the number of days associated with hazardous heat stress and thermal discomfort, particularly for Humidex ≥ 30 °C.

Following the analysis of observed trends, the future heat-stress hazard was evaluated using climate model projections. Future projections of heat-stress hazard were derived from an ensemble of five CMIP6 global climate models (CanESM, ACCESS, GFDL, MPI,

and NorESM) under two Shared Socioeconomic Pathway (SSP) scenarios: the intermediate-mitigation scenario SSP2-4.5 (forcing reaching ~4.5 W m^{-2} by 2100) and the high-emission scenario SSP5-8.5 (high forcing reaching ~8.5 W m^{-2} by 2100). The projected percentage of April–October days exceeding selected Humidex thresholds (≥30, ≥35, and ≥40 °C) for the reference period (1991–2020) and the end-of-century period (2081–2100) is presented in Figure 6 across all five models.

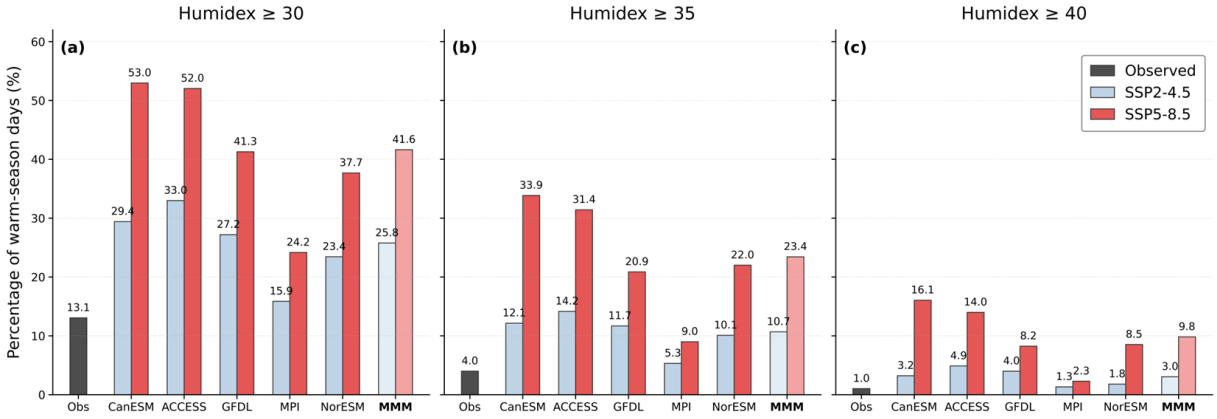

Figure 6. Projected changes in the percentage of warm-season days exceeding selected Humidex thresholds in Vilnius by the end of the 21st century. The panels show the share of April–October days with Humidex values ≥30 (**a**), ≥35 (**b**), and ≥40 (**c**) for the observed reference period and for future CMIP6 projections for 2081–2100 under SSP2-4.5 and SSP5-8.5 scenarios. Results are presented for five climate models: CanESM, ACCESS, GFDL, MPI, and NorESM, together with the multi-model mean. Bars indicate the percentage of warm-season days exceeding each threshold, with values labelled above the bars. The multi-model mean (MMM) represents the arithmetic mean of the five CMIP6 models for each scenario and Humidex threshold.

Climate model projections indicate a substantial increase in the percentage of April–October days exceeding Humidex thresholds by the end of the century (2081–2100), with higher exceedance frequencies projected under SSP5-8.5 than under SSP2-4.5 (Figure 6). For Humidex ≥ 30 °C, the observed reference-period value was 13.1%, while the projected multi-model mean, calculated as the arithmetic mean of the five CMIP6 models used in this study, reached 25.8% under SSP2-4.5 and 41.6% under SSP5-8.5, equivalent to 2.0 and 3.2 times the observed value, respectively. For Humidex ≥ 35 °C, the observed value was 4.0%, compared with projected multi-model means of 10.7% under SSP2-4.5 and 23.4% under SSP5-8.5, corresponding to 2.7 and 5.9 times the observed value. The strongest relative increase was projected for Humidex ≥ 40 °C, for which the observed value was 1.0%, while the projected multi-model means reached 3.0% under SSP2-4.5 and 9.8% under SSP5-8.5. Overall, these results indicate a pronounced increase in future heat-stress frequency in Vilnius, particularly under the high-emission scenario and for more severe Humidex exceedances.

3.2. Spatial Distribution and Population Burden of CLIMADA-Modelled Heat-Stress Risk

Figure 7 presents the spatial distribution of CLIMADA-modelled mean annual heat-stress EAI across Vilnius city municipality for 2001–2020, based on observational meteorological data. EAI values are shown only for grid cells with population exposure, while white grid cells represent areas without exposed population in the input exposure layer and were not assigned impact values. The absolute EAI map (Figure 7a) shows that the highest modelled impacts are concentrated in the central and densely populated parts of Vilnius, reflecting the strong influence of exposed population size on total heat-stress burden. In contrast, the population-normalised EAI map (Figure 7b) shows modelled

impact per 100 inhabitants and therefore reduces the dominance of highly populated grid cells. However, spatial differences remain after normalisation because EAI was calculated using age-specific exposure data and vulnerability functions. Consequently, grid cells with a higher proportion of residents aged ≥ 65 years tend to show elevated normalised EAI values due to the higher heat-stress sensitivity assigned to this age group. Thus, the two maps provide complementary perspectives on the spatial impact of heat stress: absolute EAI identifies areas with the greatest total modelled burden, whereas population-normalised EAI highlights areas where the relative burden remains elevated after accounting for differences in exposed population size.

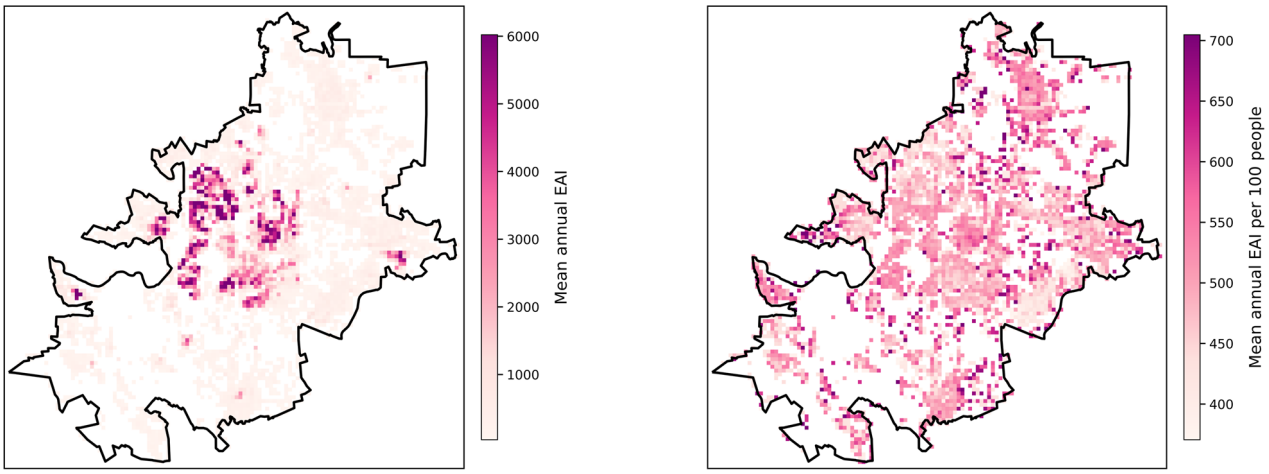

(**a**) (**b**)

Figure 7. Spatial distribution of the mean annual heat-stress burden indicator (EAI) in Vilnius city municipality for 2001–2020, based on observed meteorological data from Trakų Vokė meteorological station. Map (**a**) shows the absolute mean annual EAI, and map (**b**) shows the mean annual EAI normalised per 100 inhabitants. The continuous colour scales show relative spatial variation in EAI and do not represent validated low, medium, or high burden categories.

Figure 8 compares the spatial distribution of heat-stress EAI during the observational reference period with end-of-century projections under the SSP5-8.5 scenario. The five CMIP6 models used in this study indicate higher future EAI values, showing a substantial increase in modelled heat-stress burden by 2081–2100. Because the spatial structure of the exposure layer is retained, the main locations of elevated EAI remain broadly consistent with the observational baseline. Differences between the reference and future maps, therefore, primarily reflect changes in projected heat-stress hazard, together with changes in total population size and age-group composition within grid cells, rather than a relocation of exposed population. Population-normalised EAI retains a broadly similar spatial distribution across the future projections, but its magnitude increases within the same populated grid cells. The magnitude of the increase varies across models, with ACCESS and CanESM showing the strongest increases, GFDL and NorESM showing intermediate responses, and MPI indicating the lowest projected impact.

While Figure 8 illustrates the spatial distribution of EAI for the end-of-century period under the high-emission SSP5-8.5 scenario, Table 1 provides a broader quantitative comparison across both SSP2-4.5 and SSP5-8.5 and for the mid-century (2041–2060) and end-of-century (2081–2100) periods. The table reports the mean annual EAI, normalised per exposed person, for the <65 and ≥65 age groups, enabling the projected heat-stress burden to be compared across age groups, scenarios, periods, and climate models. The corresponding inter-model population standard deviations are also presented to quantify the spread across the five selected CMIP6 model-based EAI projections.

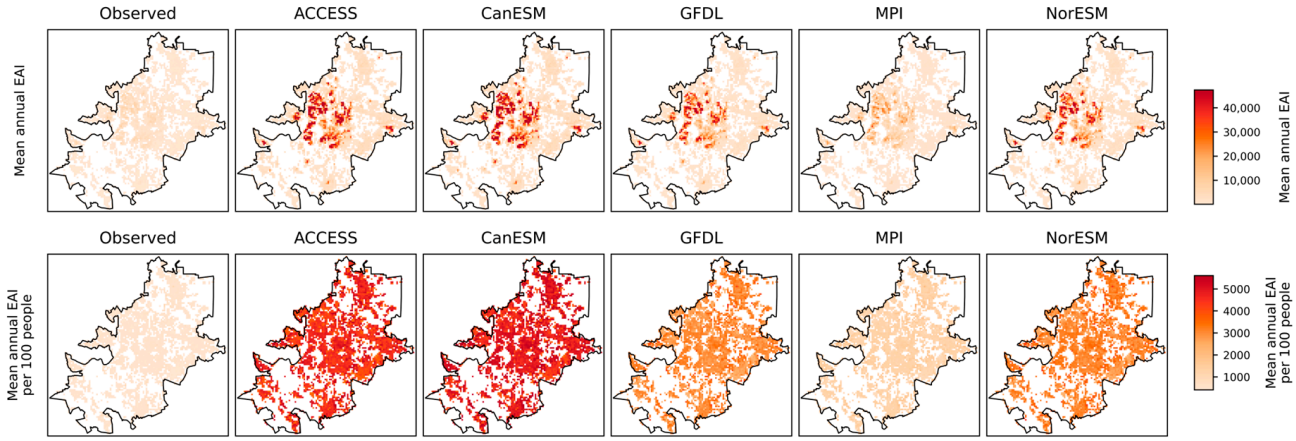

Figure 8. Spatial distribution of the mean annual heat-stress burden indicator (EAI) in Vilnius city municipality for the historical reference period 2001–2020 and future CMIP6 SSP5-8.5 projections for 2081–2100. The columns show the LHMS observational dataset and five climate model projections: ACCESS, CanESM, GFDL, MPI, and NorESM. The upper row presents absolute mean annual EAI values, while the lower row presents mean annual EAI normalised per 100 inhabitants. The continuous colour scales show relative spatial variation in EAI and do not represent validated low, medium, or high burden categories.

Table 1. Mean annual Expected Annual Impact normalised per exposed person (EAI/person/year) for the population aged < 65 years and ≥65 years in Vilnius, Lithuania, under SSP2-4.5 and SSP5-8.5 climate scenarios for 2041–2060 and 2081–2100. The <65 years group combines the 0–14 and 15–64 age groups, while the ≥65 years group represents the population aged 65 years and older. EAI values were calculated using the CLIMADA risk assessment framework for heat-stress days defined by Humidex ≥ 30 °C, and then divided by the corresponding age-group population total. The multi-model mean was calculated as the arithmetic mean of the five CMIP6 model-specific EAI values for each age group, scenario, and period. The corresponding inter-model standard deviation was calculated across the same five model-specific EAI values using the population standard deviation and is presented as a descriptive measure of model spread rather than as a confidence interval. Higher values indicate a greater average annual heat-stress burden per person within the respective age group.

Model *	Age Group	SSP2-4.5 2041–2060	SSP5-8.5 2041–2060	SSP2-4.5 2081–2100	SSP5-8.5 2081–2100
CanESM	<65 years	7.9	10.4	11.9	39.0
	≥65 years	24.6	30.5	25.1	64.6
ACCESS	<65 years	7.0	8.5	14.5	35.9
	≥65 years	22.5	26.5	29.1	60.8
GFDL	<65 years	7.3	7.5	12.0	22.4
	≥65 years	22.6	24.2	23.7	41.4
MPI	<65 years	3.6	4.5	5.2	8.8
	≥65 years	11.7	13.6	11.6	19.2
NorESM	<65 years	5.5	8.8	8.2	23.6
	≥65 years	19.1	26.7	19.4	42.9
Multi-model mean ± inter-model SD	<65 years	6.3 ± 1.5	7.9 ± 2.0	10.4 ± 3.3	25.9 ± 10.8
	≥65 years	20.1 ± 4.6	24.3 ± 5.7	21.8 ± 6.0	45.8 ± 16.2

* For comparison, the observed 2001–2020 LHMS reference values are 4.0 EAI/person/year for the population aged < 65 years and 9.1 EAI/person/year for the population aged ≥ 65 years.

For the observed 2001–2020 reference period, EAI/person/year was 4.0 for the population aged < 65 years and 9.1 for the population aged ≥ 65 years. Future projections generally exceed these reference values, particularly for the ≥65 years group. Across

all models, scenarios, and periods, EAI/person/year is consistently higher for residents aged ≥65 years than for those aged < 65 years, reflecting the greater heat-stress sensitivity assigned to older residents in the vulnerability functions.

By mid-century, the multi-model mean EAI/person/year for the <65 years group increased from the observed reference value of 4.0 to 6.3 ± 1.5 under SSP2-4.5 and 7.9 ± 2.0 under SSP5-8.5, with model ranges of 3.6–7.9 and 4.5–10.4, respectively. For the ≥65 years group, the corresponding mean values increase from the observed reference value of 9.1 to 20.1 ± 4.6 under SSP2-4.5 and 24.3 ± 5.7 under SSP5-8.5, with model ranges of 11.7–24.6 and 13.6–30.5. By the end of the century, the increase becomes more pronounced, particularly under SSP5-8.5. Under this scenario, the multi-model mean reaches 25.9 ± 10.8 EAI/person/year for the <65 years group and 45.8 ± 16.2 EAI/person/year for the ≥65 years group, equivalent to approximately 6.5 and 5.0 times the observed reference values, respectively. Across scenarios and periods, the ≥65 years group consistently shows substantially higher EAI/person/year than the <65 years group, indicating a strong age-related differentiation in projected heat-stress burden. The highest values are projected by CanESM and ACCESS, whereas MPI generally produces the lowest estimates.

The lower EAI values projected by MPI are consistent with weaker local heat-stress hazard conditions in the downscaled and bias-corrected input data. Under SSP5-8.5 in 2081–2100, MPI had a 95th-percentile maximum air temperature of 33.1 °C, compared with 33.6–38.3 °C across the other selected models, and the lowest mean relative humidity of 68.2%. Since Humidex is calculated from air temperature and relative humidity, lower air temperature and humidity conditions resulted in lower Humidex values and fewer heat-stress exceedance days, which subsequently led to lower EAI estimates. In contrast, CanESM and ACCESS generally produced stronger local heat-stress hazard conditions and correspondingly higher EAI values, while NorESM showed an intermediate response.

Figure 9 summarises the mean annual total EAI across all age groups, providing an integrated estimate of municipality-wide heat-stress burden. While the previous maps illustrate the spatial distribution of EAI and Table 1 quantifies age-specific impacts per person, Figure 9 shows how the total annual impact changes between the observed baseline and future climate projections.

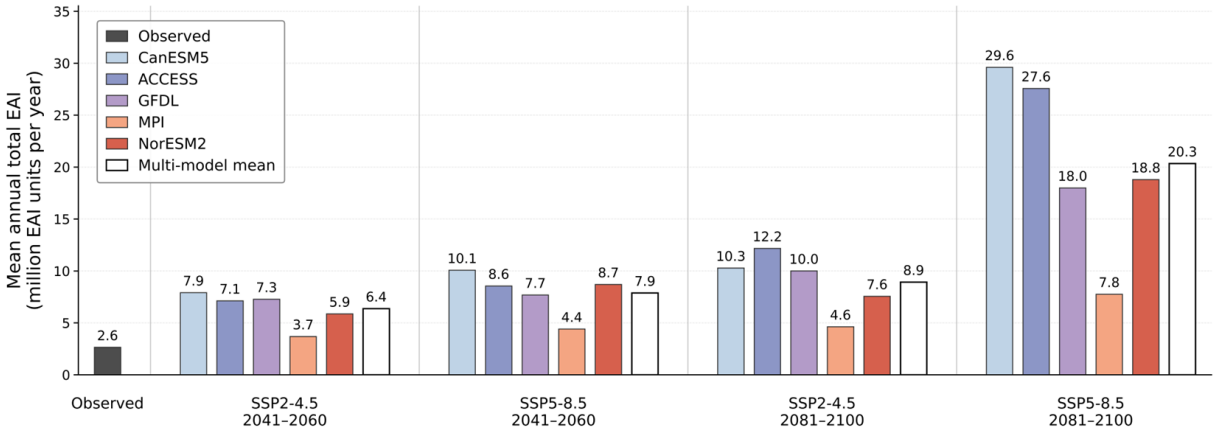

Figure 9. Mean annual total Expected Annual Impact (EAI) from heat-stress days in Vilnius for the observed period 2001–2020 and CMIP6 projections for 2041–2060 and 2081–2100 under SSP2-4.5 and SSP5-8.5. Values are scaled by 10^6 EAI year^{-1} and represent the total annual heat-stress burden across all age groups. Colours indicate individual climate models, grey denotes the observed baseline, and the multi-model mean represents the arithmetic mean of the five CMIP6 models for each scenario and period.

The observed mean annual EAI for 2001–2020 was 2.6×10^6 EAI year^{-1}. For 2041–2060, projected values increased from 3.7×10^6 to 7.9×10^6 EAI year^{-1} under SSP2-4.5 and from 4.4×10^6 to 10.1×10^6 EAI year^{-1} under SSP5-8.5. By 2081–2100, the increase became more pronounced, with EAI ranging from 4.6×10^6 to 12.2×10^6 EAI year^{-1} under SSP2-4.5 and from 7.8×10^6 to 29.6×10^6 EAI year^{-1} under SSP5-8.5. The highest end-of-century impacts were projected by CanESM and ACCESS, whereas MPI consistently produced the lowest estimates.

A sensitivity analysis of the vulnerability-function parameterization was performed by varying H_{50} and n independently by ±5% while keeping all other model inputs unchanged (Figure 10). The analysis shows that EAI/person/year is much more sensitive to changes in H_{50} than to changes in n.

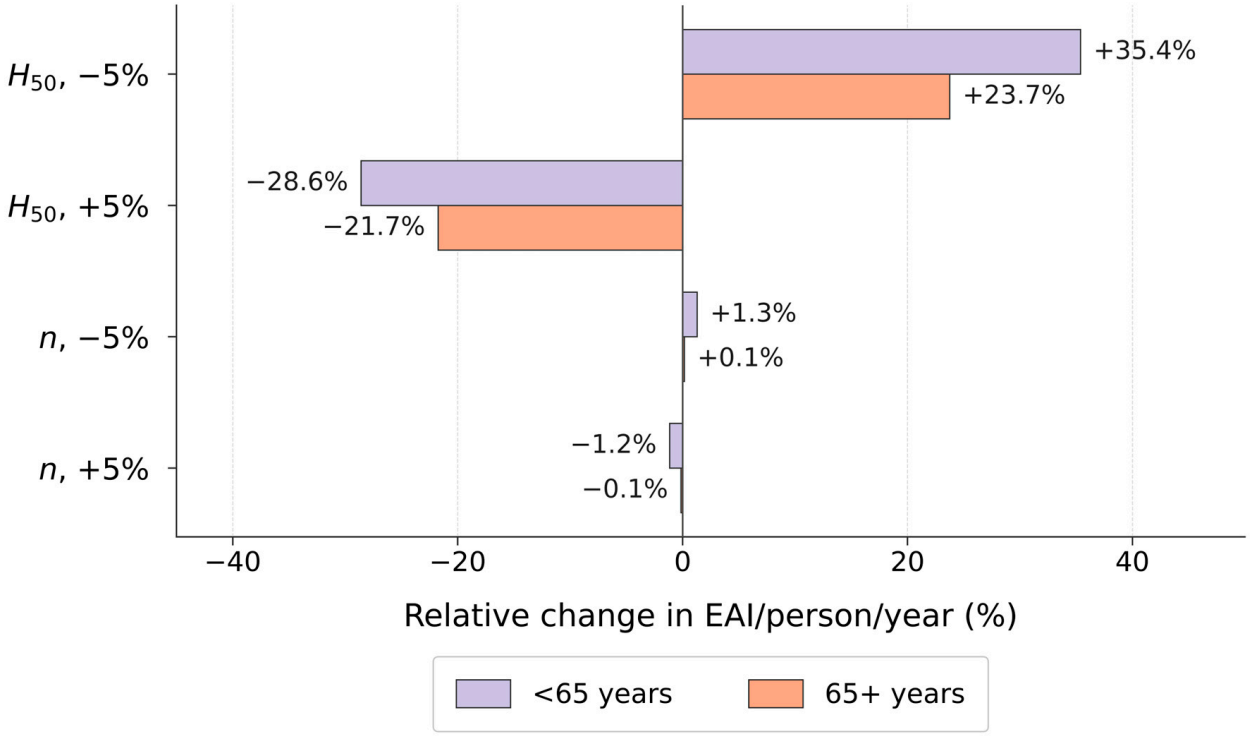

Figure 10. Sensitivity analysis of mean annual Expected Annual Impact normalised per exposed person (EAI/person/year) by age groups. The bars show the relative change in EAI/person/year when either vulnerability-function parameter was increased or decreased by 5% from its baseline value. H_{50} represents the Humidex level associated with a 50% heat-stress impact, while n determines the steepness of the vulnerability function. Results are shown for the end of the century (2081–2100) SSP5-8.5 scenario multi-model mean. The multi-model mean represents the arithmetic mean of the five CMIP6 model-specific EAI values.

The larger relative sensitivity for the population aged < 65 years partly reflects the different baseline H_{50} values used for the two age groups, with the ±5% changes calculated from H_{50} = 40 for the population aged < 65 years and H_{50} = 36 for the population aged 65+ years. In addition, the effect of changing H_{50} depends on its position relative to the distribution of Humidex values, with larger changes occurring when a greater proportion of heat-stress events falls within the steepest part of the vulnerability function. These results indicate that the selection of H_{50} can substantially influence the estimated heat-stress impact and should therefore be carefully considered when defining vulnerability functions.

4. Discussion

4.1. Main Findings and Historical Trends

The primary findings of this Vilnius heat-risk assessment demonstrate a substantial increase in Humidex-based heat-stress conditions during the historical period and further intensification under future climate scenarios. Observational data for 1991–2024 confirm that heat-stress intensification is already underway, with statistically significant increases across all assessed Humidex thresholds, including a +5.57-day-per-decade increase for Humidex $\geq$ 30 °C. Spatial analysis indicates that heat-stress burden is unevenly distributed across Vilnius, with higher modelled impacts concentrated in densely populated urban areas where elevated Humidex-derived hazard coincides with greater population exposure. The CLIMADA-based impact estimates show that cumulative heat-stress burden, expressed as EAI, could increase by approximately 1.8–11.4 times relative to the historical baseline by 2081–2100, depending on the emissions scenario and climate model. Together, these findings indicate that future urban heat-stress risk in Vilnius is shaped not only by increasing thermal hazard, but also by the spatial distribution and demographic vulnerability of the exposed population.

The historical trend analysis indicates that the most pronounced changes in Vilnius occurred at Humidex thresholds associated with some-to-moderate thermal discomfort, particularly Humidex $\geq$ 30 °C and $\geq$35 °C. This suggests that the observed increase in heat-stress burden is primarily associated with a higher frequency of warm-season exceedance days, rather than being driven exclusively by rare extreme Humidex events. Within the heat-stress risk framework, such changes are important because cumulative impact can increase substantially when moderate heat-stress conditions repeatedly affect exposed population grids, even if the highest Humidex categories remain relatively infrequent. The statistically significant upward tendencies at Humidex $\geq$ 40 °C and $\geq$45 °C further indicate that more severe heat-stress conditions are also emerging in Vilnius. Although the present study applies Humidex, this pattern is consistent with broader WBGT-based evidence showing increasing summer humid-heat extremes across Europe and identifying temperature increases as an important driver of these trends [45,46].

The projected changes identified for Vilnius are consistent with results from studies conducted in other regions of the world, which most often indicate that the frequency and intensity of urban heat stress will increase in the future. Although the magnitude of projected changes varies across cities due to differences in climate, urbanisation rates, and urban environmental conditions, the overall trend—an increasing risk of urban heat stress—is similar [47,48].

4.2. Climate Model Discrepancies

All five CMIP6-based EAI projections show an increase relative to the historical period, indicating a consistent direction of change across the selected ensemble. However, future EAI projections show that the magnitude of the heat-stress burden is sensitive to the selected climate model and therefore remains uncertain. The five CMIP6 models were selected to span different equilibrium climate sensitivities, thereby representing a range of possible climate responses within the ensemble [36]. This selection was intended to capture inter-model uncertainty in the projected temperature and humidity inputs and the resulting EAI values rather than to identify a single best-performing model. However, the resulting EAI values do not follow a simple ranking based solely on equilibrium climate sensitivity. While CanESM and ACCESS generally produce the highest end-of-century heat-stress burdens, MPI consistently gives the lowest estimates, and the relative ordering of the intermediate models varies across scenarios and periods. The differences in the outputs of the selected CMIP6 models are determined not only by equilibrium climate sensitivity

but also by model-specific regional differences in projected temperature and humidity responses, arising from both atmospheric circulation representation and differences in the parameterisation of processes across models. Since Humidex depends on both air temperature and humidity, inter-model differences in the simulation of these variables contribute to the spread of projected EAI values. This supports the interpretation that the model-dependent EAI differences observed here should be attributed not solely to equilibrium climate sensitivity, but also to model-specific regional warming and humidity responses that influence the projected Humidex hazard [49,50]. Therefore, the selected models were chosen to represent a range of plausible future climate responses rather than to provide an exact forecast for Vilnius, and the projected impacts should be interpreted accordingly as a range of possible outcomes. Although all five model-based EAI projections indicate the same direction of change, the magnitude of the projected EAI differ among models. Table 1 presents the multi-model means and corresponding inter-model standard deviations, providing a quantitative summary of the inter-model spread and enabling assessment of the consistency of the projected changes across the selected ensemble.

4.3. Spatial Patterns and Methodological Contribution

A further contribution of this study is the explicit representation of intra-urban heat-stress variability within a city-scale risk-assessment framework. Previous Lithuanian heat-related climate studies have used meteorological observations, climate projections, and, in some cases, satellite-derived land-surface temperatures to assess heatwaves, climate threats, and urban surface thermal patterns [3,27,30,51]. However, these studies used different indicators, datasets, and spatial scales and therefore do not provide directly comparable projections of Humidex frequency for Vilnius. Meteorological observations and climate projections are suitable for evaluating long-term trends and broad-scale climate signals, but are less able to resolve neighbourhood-scale variation in urban heat exposure. This study, therefore, uses UrbClim-derived near-surface air-temperature fields to represent intra-urban variation in the Humidex-based heat-stress hazard at higher spatial resolution. By linking this hazard with gridded population exposure and age-specific vulnerability, the resulting EAI maps show how projected heat-stress burden varies spatially across exposed urban populations. The interpretation of these spatial patterns is nevertheless constrained by the relatively short 2008–2017 UrbClim period and by the assumption that the temperature and humidity anomaly patterns remain unchanged under future climate conditions. However, it is important to note that the projections presented reflect potential changes due to climate change, assuming the city's morphology remains unchanged and excluding future urban expansion or adaptation measures.

Compared with previous studies, the proposed approach provides an integrated assessment of heat-stress risk by combining high-resolution hazard information with spatial exposure and age-specific vulnerability. This enables simultaneous evaluation of spatial patterns and differences among population groups under future climate scenarios.

4.4. Exposure, Vulnerability, and Population-Group Results

The exposure assumptions used in this study are important for interpreting the spatial risk results. The gridded population data provide a consistent representation of residential exposure, but do not fully capture where people are located during hot days. Daily mobility, commuting, school and workplace locations, transport use, outdoor activities, and time spent in public spaces can shift heat exposure away from residential grid cells. Recent studies have used mobile phone data, GPS tracking, and time-activity surveys to show how actual daytime heat exposure can differ from residence-based metrics [52–56]. For example, mobility-based studies have demonstrated that urban activity patterns change

during extreme heat events [54,56], while dynamic thermal exposure indices and personal monitoring approaches identify exposure hotspots based on where people actually spend time [52,53,55]. These findings suggest that residence-based exposure estimates may underrepresent daytime or activity-based heat stress, particularly in urban centres where population density and movement patterns vary strongly between day and night. In addition, outdoor Humidex conditions do not directly translate into individual heat exposure because people may spend much of the day indoors, and indoor thermal conditions depend on building type, window placement, residents' thermal conditions, and residents' influence and behaviour [57]. Future exposure is also uncertain because long-term population projections at city and neighbourhood scales are limited. In this study, the total population of Vilnius was therefore kept constant after 2025, and the relative spatial distribution of population was preserved from the 2021 grid. This assumption improves comparability between time periods, but it does not capture future urban development, residential relocation, densification, or changes in daily mobility. The resulting EAI values should therefore be interpreted as a residential-based cumulative impact indicator of heat-stress burden, rather than as actual estimates of individual exposure throughout the day or the number of affected individuals.

The age-based results highlight the importance of considering heat-stress risk as a direct burden on exposed populations, rather than only as a driver of specific health or economic outcomes. Previous studies have commonly evaluated heat impacts through direct health outcomes, including heat-related mortality and hospital admissions [4,21,24,26,29,51,58], as well as economic outcomes such as occupational productivity losses and reductions in working hours [22,23]. These approaches are important, but they do not fully capture the broader population risk of repeated thermal discomfort and heat stress in urban environments. In this study, EAI provides a generalised indicator of cumulative heat-stress burden, showing how repeated exposure to thermal discomfort can affect population groups, even when direct health outcomes are not modelled.

The higher modelled burden among residents aged 65 years and older reflects the age-based vulnerability functions used in this study and is consistent with evidence that older adults are generally more sensitive to heat exposure due to physiological, health-related, and mobility factors [4,24,59,60]. Children are also recognised as a heat-vulnerable group, but their sensitivity varies considerably across the 0–14 year age range [24,61,62]. Therefore, grouping children with the working-age population should be interpreted as a modelling simplification for estimating the generalised heat-stress burden, rather than as evidence of equivalent heat sensitivity. More broadly, individual heat response also depends on health status, housing conditions, access to cooling, occupation, behaviour, and acclimatisation. The vulnerability functions used here should therefore be viewed as population-level approximations that support comparisons between age groups and spatial areas but do not capture the full variability in individual heat tolerance or adaptive capacity.

In addition, currently, there are no established methods for measuring overall heat-stress vulnerability. The sigmoid functions used in this research were derived from studies on heat-related deaths, heat stress, and reductions in working capacity. They should be understood as theoretical, scenario-based components of the proposed risk-assessment framework, designed to support relative comparisons across age groups, locations, and climate scenarios, rather than as calibrated functions for predicting a specific outcome. The estimated EAI is sensitive to the choice of H_{50} and steepness parameters, as these determine when vulnerability begins to increase substantially and how rapidly the response develops. The sensitivity analysis showed that changes in H_{50} substantially affected the magnitude of EAI, whereas changes in n had only a minor effect. However, the relative difference between the age groups remained consistent, with higher EAI/person/year values for the

population aged 65+ years. For this reason, the values reported here should be interpreted as comparative indicators of potential impact and not as fixed, universal, or clinically validated estimates. As more solid empirical data emerge, it is important to calibrate these functions, test them under different parameter assumptions, and broaden their scope to more accurately reflect children and other populations at risk.

4.5. Implications for Municipal Adaptation

The results of this study can support municipal climate change adaptation planning by identifying areas with relatively higher modelled heat-stress burden under the current urban structure. The heat-stress burden maps can be used as a screening tool to help prioritise locations for further local assessment and adaptation planning. In higher-burden areas, plans can be developed to expand green infrastructure, increase tree canopy cover, create shade, and implement other measures to mitigate the urban heat island effect. The results can also be used to plan targeted public health measures for the most vulnerable population groups, particularly older adults. However, the maps do not account for future urban expansion, densification or the effects of planned adaptation measures. They should therefore be interpreted as climate-driven projections under the current urban structure rather than as forecasts of future urban conditions. The proposed methodological approach can be regularly updated using new climate scenarios, population data, and information on implemented adaptation measures, thereby providing a basis for a long-term process of climate risk monitoring and management.

4.6. Study Limitations

Several limitations should be considered when interpreting the results. The EAI metric represents a modelled indicator of cumulative heat-stress burden and should not be interpreted as the actual number of affected individuals or as a direct estimate of mortality, morbidity, hospital admissions, labour productivity losses, or economic damage. In addition, EAI should be interpreted as a comparative, cumulative burden indicator rather than as one with predefined impact thresholds or empirically validated EAI burden classes. Although useful for comparing relative risk across scenarios, models, age groups, and spatial units, this type of indicator may be less intuitive to stakeholders who require outcome-based metrics for decision-making.

Exposure and vulnerability were also necessarily simplified. Residential population data do not fully represent daily mobility or indoor exposure. In addition, since long-term population projections for Vilnius are unavailable, the study assumed a constant population size and distribution after 2025. This assumption allowed the study to isolate the effects of climate change, although it does not account for possible future demographic and urban changes. To analyse these changes, additional research utilising specific demographic and urban development scenarios would be necessary, but this was not within the study's current scope. In this assessment, population age was the primary vulnerability indicator because high-resolution socioeconomic data (e.g., income, housing) was unavailable for Vilnius. Consequently, the findings represent age-related vulnerability rather than a comprehensive measure of overall social vulnerability. Age-based vulnerability functions do not capture the full range of social, health, housing, occupational, and behavioural factors that influence individual heat sensitivity. The vulnerability functions used in this study should not be regarded as fixed, universal, or fully validated representations of heat-stress impacts. Although the parameter sensitivity analysis provides an initial assessment of the influence of H_{50} and steepness assumptions, it does not replace empirical calibration or validation. Because such functions are essential for risk assessments, future research should focus on their systematic calibration and validation testing using detailed health,

mortality, hospital-admission, occupational, demographic, and socioeconomic data. These efforts would strengthen the scientific basis and practical reliability of future heat-stress risk assessments.

The current study assumed that the spatial pattern of the Vilnius urban heat island remained constant over time, and it did not account for how climate change, droughts, or new urban development might alter the heat island's size and intensity. Future urban expansion, densification, changes in construction materials, surface properties, and vegetation cover could alter the intensity and spatial pattern of the urban heat island. Future urban changes could influence local thermal conditions and the intensity of the heat island, depending on the type of development and the measures implemented. These urban development and adaptation processes were not included in this framework. To address this limitation, future research should combine transient urban climate simulations with realistic urban growth and adaptation scenarios to show how the urban heat island will actually evolve.

Although additional CMIP6 models could have been included, the selected ensemble was sufficient to demonstrate the proposed framework and illustrate inter-model uncertainty. Where appropriate validation criteria are available, performance-based model selection or weighting could also be applied to develop more regionally representative future scenarios.

The use of Humidex provides a consistent basis for assessing temperature and humidity-driven heat stress, but it does not explicitly account for radiation, wind, or activity level, which may affect comparisons with studies using other thermal indices. Compound risks, including interactions between heat, air pollution, drought and pluvial flooding, were also outside the scope of the present study. Addressing these aspects in future research would strengthen the framework's use in identifying exposure patterns, vulnerable populations, and adaptation needs at the urban scale.

5. Conclusions

This study quantified urban heat-stress risk in Vilnius by combining Humidex-based hazard information, gridded population data, age-structured vulnerability functions, and CLIMADA impact modelling with historical observations and CMIP6 climate projections. The results indicate that future heat-stress risk in Vilnius will be driven not only by increasing thermal hazard but also by demographic ageing and the uneven spatial distribution of vulnerable populations.

The analysis shows that heat-stress conditions have intensified significantly over the historical period and are expected to increase further during the twenty-first century, with the largest increases projected for the SSP5-8.5 scenario in the late-century period. Projected EAI values indicate a substantial increase in cumulative heat-stress burden relative to the historical baseline, while differences among climate-model projections suggest that future risk estimates remain sensitive to the selected climate models. The spatial results reveal pronounced intra-urban variation in heat-stress burden. In the model, higher impacts occur where stronger Humidex conditions coincide with higher population density and a greater concentration of population groups assigned higher heat-stress vulnerability. The results for residents aged 65 years and older further underline the importance of accounting for age structure in urban heat risk modelling. Although EAI should be understood as a comparative burden metric rather than a direct estimate of observed health or economic outcomes, the framework provides spatially detailed evidence for identifying parts of the city and population groups where future heat-stress risk may become more pronounced. Future applications should improve the representation of population dynamics, indoor thermal exposure, socioeconomic vulnerability, alternative thermal indices, compound hazards, and adaptation scenarios. Overall, the study demonstrates that spatially explicit and

age-sensitive impact modelling can strengthen urban heat-risk assessment and adaptation planning in Vilnius, while also offering a transferable approach for other Lithuanian and Baltic states cities.

Author Contributions: Conceptualization, J.K. and E.R.; methodology, J.K. and E.R.; software, J.K.; validation, J.K.; formal analysis, J.K. and E.R.; investigation, J.K. and E.R.; resources, J.K. and E.R.; data curation, J.K.; writing—original draft preparation, J.K. and E.R.; visualisation, J.K. All authors have read and agreed to the published version of the manuscript.

Funding: This research received no external funding.

Institutional Review Board Statement: Not applicable.

Informed Consent Statement: Not applicable.

Data Availability Statement: The datasets used and/or analysed during the current study are available from the corresponding author upon reasonable request.

Conflicts of Interest: The authors declare no conflicts of interest.

Abbreviations

The following abbreviations are used in this manuscript:

ACCESS	Australian Community Climate and Earth-System Simulator Coupled Model version 2 (ACCESS-CM2)
CanESM	Canadian Earth System Model version 5
CMIP6	Coupled Model Intercomparison Project Phase 6
EAI	Expected Annual Impact
GFDL	Geophysical Fluid Dynamics Laboratory Climate Model version 4 (GFDL-CM4)
IPCC	Intergovernmental Panel on Climate Change
LHMS	Lithuanian Hydrometeorological Service
MDD	Mean damage degree
MPI	Max Planck Institute Earth System Model version 1.2, low resolution (MPI-ESM1-2-LR)
NorESM	Norwegian Earth System Model version 2, medium resolution (NorESM2-MM)
SSPs	Shared Socioeconomic Pathways

References

1. Martín, Y.; Paneque, P. Moving from Adaptation Capacities to Implementing Adaptation to Extreme Heat Events in Urban Areas of the European Union: Introducing the U-ADAPT! Research Approach. *J. Environ. Manag.* **2022**, *310*, 114773. [CrossRef] [PubMed]
2. Schwingshackl, C.; Daloz, A.S.; Iles, C.; Aunan, K.; Sillmann, J. High-Resolution Projections of Ambient Heat for Major European Cities Using Different Heat Metrics. *Nat. Hazards Earth Syst. Sci.* **2024**, *24*, 331–354. [CrossRef]
3. Ramanauskas, E.; Bukantis, A.; Dringelis, L.; Kaveckis, G.; Jonkutė-Vilkė, G. Climate Change and Cities of Lithuania: Threats, Problems and Prerequisites for Solution. *Urban Sci.* **2024**, *8*, 186. [CrossRef]
4. Fastl, C.; Arnberger, A.; Gallistl, V.; Stein, V.K.; Dorner, T.E. Heat Vulnerability: Health Impacts of Heat on Older People in Urban and Rural Areas in Europe. *Wien. Klin. Wochenschr.* **2024**, *136*, 507–514. [CrossRef] [PubMed]
5. Watts, N.; Amann, M.; Arnell, N.; Ayeb-Karlsson, S.; Beagley, J.; Belesova, K.; Boykoff, M.; Byass, P.; Cai, W.; Campbell-Lendrum, D.; et al. The 2020 Report of The Lancet Countdown on Health and Climate Change: Responding to Converging Crises. *Lancet* **2021**, *397*, 129–170. [CrossRef] [PubMed]
6. Jeong, I.D.; Yu, B.; Cannon, A.J. 2021 Heatwave Over Western North America: Structural Uncertainty and Internal Variability in GCM Projections of Humidex and Temperature Extremes. *Earths Future* **2024**, *12*, e2024EF004541. [CrossRef]
7. Do, H.X.; Le, T.H.; Le, M.H.; Nguyen, D.L.T.; Do, N.C. Future Changes in Hydro-Climatic Extremes across Vietnam: Evidence from a Semi-Distributed Hydrological Model Forced by Downscaled CMIP6 Climate Data. *Water* **2024**, *16*, 674. [CrossRef]
8. Williams, E.; Funk, C.; Peterson, P.; Tuholske, C. High Resolution Climate Change Observations and Projections for the Evaluation of Heat-Related Extremes. *Sci. Data* **2024**, *11*, 261. [CrossRef] [PubMed]

9. Higuera Roa, O.; Bachmann, M.; Mechler, R.; Šakić Trogrlić, R.; Reimann, L.; Mazzoleni, M.; Aerts, J.C.J.H.; Buskop, F.E.; Pirani, A.; Mysiak, J. Challenges and Opportunities in Climate Risk Assessment: Future Directions for Assessing Complex Climate Risks. *Environ. Res. Lett.* **2025**, *20*, 053003. [CrossRef]
10. Intergovernmental Panel on Climate Change. *Climate Change 2022–Impacts, Adaptation and Vulnerability*; Cambridge University Press: Cambridge, UK; New York, NY, USA, 2023; ISBN 9781009325844.
11. Aznar-Siguan, G.; Bresch, D.N. CLIMADA v1: A Global Weather and Climate Risk Assessment Platform. *Geosci. Model Dev.* **2019**, *12*, 3085–3097. [CrossRef]
12. Oasis Loss Modelling Framework. Oasis Loss Modelling Framework. Available online: https://oasislmf.org/ (accessed on 17 June 2026).
13. Paulik, R.; Horspool, N.; Woods, R.; Griffiths, N.; Beale, T.; Magill, C.; Wild, A.; Popovich, B.; Walbran, G.; Garlick, R. RiskScape: A Flexible Multi-Hazard Risk Modelling Engine. *Nat. Hazards* **2023**, *119*, 1073–1090. [CrossRef]
14. Negulescu, C.; Smai, F.; Quique, R.; Hohmann, A.; Clain, U.; Guidez, R.; Tellez-Arenas, A.; Quentin, A.; Grandjean, G. VIGIRISKS Platform, a Web-Tool for Single and Multi-Hazard Risk Assessment. *Nat. Hazards* **2023**, *115*, 593–618. [CrossRef]
15. Stalhandske, Z.; Steinmann, C.B.; Meiler, S.; Sauer, I.J.; Vogt, T.; Bresch, D.N.; Kropf, C.M. Global Multi-Hazard Risk Assessment in a Changing Climate. *Sci. Rep.* **2024**, *14*, 5875. [CrossRef] [PubMed]
16. Lüthi, S.; Aznar-Siguan, G.; Fairless, C.; Bresch, D.N. Globally Consistent Assessment of Economic Impacts of Wildfires in CLIMADA v2.2. *Geosci. Model Dev.* **2021**, *14*, 7175–7187. [CrossRef]
17. Mühlhofer, E.; Koks, E.E.; Kropf, C.M.; Sansavini, G.; Bresch, D.N. A Generalized Natural Hazard Risk Modelling Framework for Infrastructure Failure Cascades. *Reliab. Eng. Syst. Saf.* **2023**, *234*, 109194. [CrossRef]
18. Kacker, K.; Srivastava, P.; Mukherjee, M. Personalized Heat Stress Early Warning System for an Urban Area. *Environ. Int.* **2025**, *199*, 109507. [CrossRef] [PubMed]
19. Spangler, K.R.; Liang, S.; Wellenius, G.A. Wet-Bulb Globe Temperature, Universal Thermal Climate Index, and Other Heat Metrics for US Counties, 2000–2020. *Sci. Data* **2022**, *9*, 326. [CrossRef]
20. Kjellstrom, T.; Holmer, I.; Lemke, B. Workplace Heat Stress, Health and Productivity-an Increasing Challenge for Low and Middle-Income Countries during Climate Change. *Glob. Health Action* **2009**, *2*, 2047. [CrossRef] [PubMed]
21. Zitouni, D.C.; Berkouk, D.; Matallah, M.E.; Ben Ratmia, M.A.E.; Attia, S. Advancing Heat Health Risk Assessment: Hotspot Identification of Heat Stress and Risk Across Municipalities in Algiers, Algeria. *Atmosphere* **2025**, *16*, 484. [CrossRef]
22. Foster, J.; Smallcombe, J.W.; Hodder, S.; Jay, O.; Flouris, A.D.; Nybo, L.; Havenith, G. An Advanced Empirical Model for Quantifying the Impact of Heat and Climate Change on Human Physical Work Capacity. *Int. J. Biometeorol.* **2021**, *65*, 1215–1229. [CrossRef] [PubMed]
23. Dawkins, L.C.; Bernie, D.J.; Lowe, J.A.; Economou, T. Assessing Climate Risk Using Ensembles: A Novel Framework for Applying and Extending Open-Source Climate Risk Assessment Platforms. *Clim. Risk Manag.* **2023**, *40*, 100510. [CrossRef]
24. Wu, X.; Wang, J.; Ge, Y.; Lai, S.; Zhang, D.; Ren, Z.; Wang, J. Future Heat-Related Mortality in Europe Driven by Compound Day-Night Heatwaves and Demographic Shifts. *Nat. Commun.* **2025**, *16*, 7420. [CrossRef] [PubMed]
25. Dasgupta, S.; van Maanen, N.; Gosling, S.N.; Piontek, F.; Otto, C.; Schleussner, C.F. Effects of Climate Change on Combined Labour Productivity and Supply: An Empirical, Multi-Model Study. *Lancet Planet. Health* **2021**, *5*, e455–e465. [CrossRef] [PubMed]
26. Lüthi, S.; Fairless, C.; Fischer, E.M.; Scovronick, N.; Armstrong, B.; Coelho, M.D.S.Z.S.; Guo, Y.L.; Guo, Y.; Honda, Y.; Huber, V.; et al. Rapid Increase in the Risk of Heat-Related Mortality. *Nat. Commun.* **2023**, *14*, 4894. [CrossRef] [PubMed]
27. Ramanauskas, E.; Bukantis, A.; Dringelis, L.; Kaveckis, G.; Jonkutė-Vilkė, G. Urban Environment and Structure of Lithuanian Cities: Their Assessment in the Context of Climate Change and Other Potential Threats. *Land* **2025**, *14*, 1759. [CrossRef]
28. Ye, Z.; Christensen, J.H.; Geels, C.; Sandstad, M.; Schwingshackl, C.; Hodnebrog, Ø.; Iles, C.; Aunan, K.; Im, U. Regional Patterns of Heat Wave and Heat Stress Intensification across Europe from High-Resolution WRF Simulations Under SSP Scenarios. *Environ. Res. Clim.* **2025**, *4*, 035015. [CrossRef]
29. Masselot, P.; Mistry, M.N.; Rao, S.; Huber, V.; Monteiro, A.; Samoli, E.; Stafoggia, M.; de'Donato, F.; Garcia-Leon, D.; Ciscar, J.C.; et al. Estimating Future Heat-Related and Cold-Related Mortality under Climate Change, Demographic and Adaptation Scenarios in 854 European Cities. *Nat. Med.* **2025**, *31*, 1294–1302. [CrossRef] [PubMed]
30. Dailidienė, I.; Servaitė, I.; Dailidė, R.; Vasiliauskienė, E.; Rapolienė, L.; Povilanskas, R.; Valiukas, D. Increasing Trends of Heat Waves and Tropical Nights in Coastal Regions (The Case Study of Lithuania Seaside Cities). *Sustainability* **2023**, *15*, 4281. [CrossRef]
31. Šukys, J.; Kilpys, J. Characterization of Climate Change in Lithuania in 1961–2020 Using Climate Extreme Indices. *Baltica* **2025**, *38*, 182–193. [CrossRef]
32. State Data Agency Statistics Lithuania. Vilniaus Miesto Gyventojų Skaičius. Available online: https://geodata.lt/vilniaus-miesto-gyventoju-skaicius/ (accessed on 17 June 2026).
33. Mirsanjari, M.M.; Visockiene, J.S.; Mohammadyari, F.; Zarandian, A. Modelling of Expansion Changes of Vilnius City Area and Impacts on Landscape Patterns Using an Artificial Neural Network. *Ecol. Chem. Eng. S* **2021**, *28*, 429–447. [CrossRef]

34. NASA Center for Climate Simulation. NASA Earth EXchange Global Daily Downscaled Projections Version 2 (NEX-GDDP-CMIP6 v2.0). Available online: https://www.nccs.nasa.gov/data-collections/nex-gddp-cmip6/ (accessed on 17 June 2026).
35. Thrasher, B.; Wang, W.; Michaelis, A.; Melton, F.; Lee, T.; Nemani, R. NASA Global Daily Downscaled Projections, CMIP6. *Sci. Data* **2022**, *9*, 262. [CrossRef]
36. Meehl, G.A.; Senior, C.A.; Eyring, V.; Flato, G.; Lamarque, J.-F.; Stouffer, R.J.; Taylor, K.E.; Schlund, M. Context for Interpreting Equilibrium Climate Sensitivity and Transient Climate Response from the CMIP6 Earth System Models. *Sci. Adv.* **2020**, *6*, eaba1981. [CrossRef] [PubMed]
37. Souverijns, N.; Lauwaet, D.; Lejeune, Q.; Kropf, C.M.; Yeung, K.L.; Nath, S.; Schleussner, C.F. 100 m Climate and Heat Stress Data up to 2100 for 142 Cities Around the Globe. *Data Brief.* **2026**, *65*, 112497. [CrossRef] [PubMed]
38. De Ridder, K.; Lauwaet, D.; Maiheu, B. UrbClim–A Fast Urban Boundary Layer Climate Model. *Urban Clim.* **2015**, *12*, 21–48. [CrossRef]
39. Masterton, J.M.; Richardson, F.A. *Humidex: A Method of Quantifying Human Discomfort Due to Excessive Heat and Humidity*; Environment Canada, Atmospheric Environment: Downsview, ON, Canada, 1979.
40. Magnus, G. Versuche Über Die Spannkräfte Des Wasserdampfs. *Ann. Phys.* **1844**, *137*, 225–247. [CrossRef]
41. Government of Canada. How to Use the Humidex. Available online: https://www.canada.ca/en/services/environment/weather/severeweather/humidex.html (accessed on 12 July 2026).
42. Lerch, M.; Du, W.; Beckendorff, D. Internal Migration Over the Course of Urbanization in Developing Countries. *Popul. Dev. Rev.* **2025**, *51*, 1022–1046. [CrossRef]
43. Qin, X.; Yang, J. Population Growth–Decline Differentiation and Regional Inequality in the Yangtze River Delta: Implications for Sustainable Regional Development. *Sustainability* **2025**, *17*, 11011. [CrossRef]
44. Ades, A.F.; Glaeser, E.L. Trade and Circuses: Explaining Urban Giants. *Q. J. Econ.* **1995**, *110*, 195–227. [CrossRef]
45. Milrad, S.M.; Ennis, K.E. Assessing Summer Humid Heat in Europe: Trends, Extremes, and Drivers. *Int. J. Climatol.* **2025**, *45*, e8913. [CrossRef]
46. Casanueva, A.; Kotlarski, S.; Fischer, A.M.; Flouris, A.D.; Kjellstrom, T.; Lemke, B.; Nybo, L.; Schwierz, C.; Liniger, M.A. Escalating Environmental Summer Heat Exposure—A Future Threat for the European Workforce. *Reg. Environ. Change* **2020**, *20*, 40. [CrossRef]
47. Briegel, F.; Schrodi, S.; Sulzer, M.; Brox, T.; Pinto, J.G.; Christen, A. Deep Learning Enables City-Wide Climate Projections of Street-Level Heat Stress. *Urban Clim.* **2025**, *62*, 102564. [CrossRef]
48. Popp, Z.; Sue Wing, I.; Lane, K.J.; Wellenius, G.A. A US Heat Disaster? Intersection of Social Vulnerability and Temperature Extremes Exacerbated by Mid-Century Climate Change and Population Shifts. *Environ. Res. Health* **2025**, *3*, 025009. [CrossRef]
49. Kong, Q.; Huber, M. A Global High-Resolution and Bias-Corrected Dataset of CMIP6 Projected Heat Stress Metrics. *Sci. Data* **2025**, *12*, 246. [CrossRef] [PubMed]
50. Lutsko, N.J. The Relative Contributions of Temperature and Moisture to Heat Stress Changes under Warming. *J. Clim.* **2021**, *34*, 901–917. [CrossRef]
51. Martinez, G.S.; Diaz, J.; Hooyberghs, H.; Lauwaet, D.; De Ridder, K.; Linares, C.; Carmona, R.; Ortiz, C.; Kendrovski, V.; Adamonyte, D. Cold-Related Mortality vs Heat-Related Mortality in a Changing Climate: A Case Study in Vilnius (Lithuania). *Environ. Res.* **2018**, *166*, 384–393. [CrossRef] [PubMed]
52. Huang, X.; Jiang, Y.; Mostafavi, A. The Emergence of Urban Heat Traps and Human Mobility in 20 US Cities. *npj Urban Sustain.* **2024**, *4*, 6. [CrossRef]
53. Milando, C.W.; Black-Ingersoll, F.; Heidari, L.; López-Hernández, I.; de Lange, J.; Negassa, A.; McIntyre, A.M.; Martinez, M.P.B.; Bongiovanni, R.; Levy, J.I.; et al. Mixed Methods Assessment of Personal Heat Exposure, Sleep, Physical Activity, and Heat Adaptation Strategies among Urban Residents in the Boston Area, MA. *BMC Public Health* **2022**, *22*, 2314. [CrossRef] [PubMed]
54. Renninger, A.; Cabrera, C. Extreme Heat Reduces and Reshapes Urban Mobility. *PNAS Nexus* **2026**, *5*, pgag078. [CrossRef] [PubMed]
55. Yin, Y.; Grundstein, A.; Mishra, D.R.; Ramaswamy, L.; Hashemi Tonekaboni, N.; Dowd, J. DTEx: A Dynamic Urban Thermal Exposure Index Based on Human Mobility Patterns. *Environ. Int.* **2021**, *155*, 106573. [CrossRef] [PubMed]
56. Tian, H.; Cai, H.; Hu, L.; Qiang, Y.; Zhou, B.; Yang, M.; Lin, B. Unveiling Community Adaptations to Extreme Heat Events Using Mobile Phone Location Data. *J. Environ. Manag.* **2024**, *366*, 121665. [CrossRef] [PubMed]
57. Lundgren Kownacki, K.; Gao, C.; Kuklane, K.; Wierzbicka, A. Heat Stress in Indoor Environments of Scandinavian Urban Areas: A Literature Review. *Int. J. Environ. Res. Public Health* **2019**, *16*, 560. [CrossRef] [PubMed]
58. Vaghefi, A.S.; Bucher, I.; Senni, C.C.; Muccione, V.; Ragettli, M.S.; Mirmashhouri, A.; Huggel, C.; Leippold, M. Quantifying the Financial Burden of Heat-Related Hospital Admissions in Switzerland under a Changing Climate: A Scalable Analytical Framework. *BMC Glob. Public Health* **2026**, *4*, 52. [CrossRef] [PubMed]
59. Vanos, J.; Guzman-Echavarria, G.; Baldwin, J.W.; Bongers, C.; Ebi, K.L.; Jay, O. A Physiological Approach for Assessing Human Survivability and Liveability to Heat in a Changing Climate. *Nat. Commun.* **2023**, *14*, 7653. [CrossRef] [PubMed]

60. Foster, J.; Hodder, S.G.; Lloyd, A.B.; Havenith, G. Individual Responses to Heat Stress: Implications for Hyperthermia and Physical Work Capacity. *Front. Physiol.* **2020**, *11*, 541483. [CrossRef] [PubMed]
61. Van de Kamp, E.; Daanen, H. Narrative Review on Infants' Thermoregulatory Response to Heat. *Int. J. Environ. Res. Public Health* **2025**, *22*, 1265. [CrossRef] [PubMed]
62. Morrison, S.A. Moving in a Hotter World: Maintaining Adequate Childhood Fitness as a Climate Change Countermeasure. *Temperature* **2023**, *10*, 179–197. [CrossRef] [PubMed]

Disclaimer/Publisher's Note: The statements, opinions and data contained in all publications are solely those of the individual author(s) and contributor(s) and not of MDPI and/or the editor(s). MDPI and/or the editor(s) disclaim responsibility for any injury to people or property resulting from any ideas, methods, instructions or products referred to in the content.